

Rate-Power Tradeoff in THz SWIPT Systems Employing Resonant Tunnelling Diode-based EH Circuits

Nikita Shanin, Simone Clochiatti, Kenneth M. Mayer, Laura Cottatellucci, Nils Weimann, and Robert Schober

Abstract

In this paper, we study terahertz (THz) simultaneous wireless information and power transfer (SWIPT) systems. Since coherent information detection is challenging at THz frequencies and Schottky diodes may not be efficient for THz energy harvesting (EH) and information detection, we employ unipolar amplitude shift keying (ASK) modulation at the transmitter (TX) and a resonant tunnelling diode (RTD)-based EH circuit at the receiver (RX) to extract both information and power from the RX signal. We model the dependence of the instantaneous output power at the RX on the instantaneous received power by a non-linear piecewise function, whose parameters are adjusted to fit circuit simulation results. To determine the rate-power tradeoff in THz SWIPT systems, we derive the distribution of the TX signal that maximizes the *mutual information* between the TX and RX signals subject to constraints on the required average harvested power at the RX and the peak signal amplitude at the TX. Since the computational complexity of maximizing the mutual information may be too high for real-time THz SWIPT systems, for high and low required average harvested powers, we also obtain the suboptimal input signal distribution that maximizes the *achievable information rate* numerically and in closed form, respectively. Furthermore, based on the obtained results, we propose a suboptimal closed-form TX distribution which also achieves a desired harvested power at the RX. Our simulation results show that a lower reverse current flow and a higher breakdown voltage of the employed RTD are preferable when the input signal power at the RX is low and high, respectively. Furthermore, we show that all proposed input distributions yield practically identical SWIPT system performance. Finally, we demonstrate that for low and high received signal powers, the rate-power tradeoff of THz SWIPT systems is determined by the peak amplitude of the TX signal and the maximum instantaneous harvested power, respectively.

This paper was submitted in part to the IEEE Global Communications Conference, 2023 [1].

Index Terms

Terahertz communications, non-linear energy harvesting, resonant tunnelling devices, signal design.

I. INTRODUCTION

Micro-scale terahertz (THz) Internet-of-Things (IoT) networks are one of the most important use cases of future sixth-generation (6G) communication systems [2]. In these networks, microscopic low-power IoT devices communicate at extremely high aggregate data rates exceeding 100 Gbit s^{-1} , which are enabled by the huge available spectrum in the THz frequency band. One unsolved problem, which hinders the design of truly micro-scale IoT devices, is the need to regularly replace their batteries [3]. A promising solution to this non-trivial problem is simultaneous wireless information and power transfer (SWIPT), where both information and power are transmitted in the downlink making battery replacement at the user devices obsolete [4]–[15].

The theoretical limits of SWIPT were first analysed in [4], where the author showed that, for discrete-time SWIPT systems, there exists a fundamental tradeoff between the information rate and the power harvested at a user device. This tradeoff can be characterized by a rate-power region, whose boundary is defined by the input signal distributions maximizing the information rate for given required average harvested powers at the user device. The rate-power tradeoff of practical SWIPT systems was studied in [5], where the authors considered time-sharing and power-splitting between energy harvesting (EH) and information detection at the receiver (RX). Furthermore, in [6], the authors characterized the performance of EH-based THz communication systems, where a relay node was utilized to overcome the huge path-loss of THz channels, and thus, to improve the data rate. Moreover, since the number of scatterers in THz wireless channels is limited [2] and a line-of-sight (LoS) between transmitter (TX) and RX may not always be available [3], the authors in [7] investigated optimal resource allocation for SWIPT systems employing intelligent reflecting surfaces (IRSs) to bypass blockages.

In designing SWIPT systems in [4]–[7], the authors assumed a linear relationship between the received and the harvested powers. However, the experimental results in [8] revealed that practical electrical circuits utilized for EH exhibit a highly non-linear behaviour. In fact, due to the non-linear current-voltage (I-V) characteristic of EH rectifying diodes, the power harvested by EH circuits can not be accurately characterized by a linear function of the received signal

power [8], [9]. Furthermore, when the input power at the EH device is high, the EH circuit is driven into saturation due to the breakdown of the employed diode [9]. To take the non-linear behaviour of EH circuits into account, in [10]–[15], the authors utilized non-linear EH models for the design of EH-based communication networks. In particular, the authors of [10] proposed an EH model based on a parametrized sigmoidal function to describe the dependence between the *average* harvested power and the *average* input power at the EH node. The parameters of the EH model in [10] were adjusted to fit circuit simulation results assuming a Gaussian waveform for the transmit signal. The EH model in [10] was widely utilized for the design of EH-based communication networks, incorporating, e.g., eavesdroppers [11], relays [12], and IRSs [13].

We note that for the EH model proposed in [10] and utilized in [11]–[13], a TX signal with fixed and known waveform is assumed. To optimize the TX waveform for SWIPT, the authors of [14] analyzed an EH circuit based on a Schottky diode and derived a corresponding closed-form EH model to characterize the *instantaneous* power harvested at the user device as a function of the *instantaneous* received signal power. Utilizing the proposed circuit-based EH model, the authors of [14] studied SWIPT systems with separate energy and information RXs, and similar to [4], determined the optimal transmit signal distribution that maximizes the mutual information between the TX signal and the signal received at the information RX under a constraint on the average harvested power at an EH node. Finally, since practical IoT sensors may require both information and power, the authors of [15] determined the optimal input distribution for SWIPT systems, where the EH node and the information RX were collocated in the same device. In contrast to [5], the information and energy RXs in [15] were connected to different antennas, and thus, could operate simultaneously without splitting the RX power.

Although the EH models in [14] and [15] accurately characterize the instantaneous harvested power for Schottky diode-based EH circuits, they may not be suitable for signal design for SWIPT systems operating in the THz frequency band. In fact, not only the characteristics of the wireless communication channels, but also the properties of the utilized electronic devices vary with frequency. In contrast to Schottky diodes, whose reverse recovery time is typically large, ~ 100 ps, resonant tunnelling diodes (RTDs) featuring a potential well and multiple quantum barriers have transient times of less than 1 ps, which allow them to operate for frequencies of up to 2 THz [16], [17]. Furthermore, RTDs typically have a smaller form factor and a larger curvature at the zero-bias point compared to Schottky diodes, and thus, lend themselves to integration with THz on-chip antennas and application in microscopic IoT devices [18]. The experiments

in [16] revealed that due to an added tunnelling current in a narrow biasing window, the I-V forward-bias characteristic of RTDs is not only highly non-linear, but also exhibits multiple critical points, a region of negative resistance, and a dependence on the signal frequency [18]. Moreover, when driven into the region of negative resistance, the RTD may self-oscillate and act as a resonant self-mixing device [18]. Thus, RTDs differ in their behaviour substantially from Schottky diodes which exhibit static and monotonic I-V characteristics [19]. Furthermore, the quality of signal rectification by EH circuits depends not only on the forward-bias I-V characteristic of the employed diode, but also on the diode breakdown voltage and reverse leakage current, which are different for RTDs and Schottky diodes [16], [20]. Although a complete and accurate model capturing the frequency dependence, non-linearity, and non-monotonicity of the current flow through RTDs is not available yet, in [16] and [17], the authors developed a compact Keysight ADS [21] model for RTDs, which is based on spline approximation and fits the measurement data presented in [16] for a wide range of operating frequencies.

Finally, unlike for SWIPT systems operating in the gigahertz (GHz) frequency band, the design of coherent information RXs, which detect the phase of the received THz signal, is challenging due to the instability and phase noise of THz local oscillators [22]. However, since the spectrum available in the THz band is significantly larger compared to that in the GHz frequency band, high data rates can also be achieved with unipolar amplitude shift keying (ASK) modulation [22]. Furthermore, since EH circuits are envelope detectors, they can not only harvest energy, but can also be exploited for extracting information from the received THz signal if unipolar ASK modulation is utilized. Moreover, since, in THz communication, the required data rates are high and the channel time coherence intervals are small, computationally complex THz signal processing algorithms may not be feasible in practice and low-complexity waveform designs are needed for THz SWIPT systems [2], [3].

In [1], which is the conference version of this paper, we characterized the achievable information rate of THz SWIPT systems employing the RTD design in [16]. In this work, we investigate the rate-power region and derive TX signal distributions maximizing the mutual information and achievable rate for THz SWIPT systems taking into account all non-linear characteristics of the employed RTD-based RX circuits. To this end, we consider a single-user THz SWIPT system employing a highly directive antenna and unipolar ASK modulation at the TX, and an RTD-based EH circuit at the RX to extract both information and energy from the received THz signal. The main contributions of this paper can be summarized as follows.

- To characterize the instantaneous power of the output signal at an RTD-based RX, we propose a general non-linear piecewise EH model, whose parameters are adjusted to fit circuit simulation results. To investigate the impact of various RTD characteristics on SWIPT system performance, in contrast to [1], we consider not only the RTD developed in [16], but also two improved RTD designs with a lower reverse leakage current and a higher breakdown voltage, respectively.
- To determine the rate-power region of THz SWIPT systems, we formulate an optimization problem for the maximization of the mutual information between the TX and RX signals subject to constraints on the average harvested power at the RX and the peak amplitude of the TX signal. We provide a feasibility condition for the problem and derive the TX signal distribution that solves the formulated problem.
- Since the computational complexity of maximizing the mutual information may be high, for high and low required average harvested powers, we not only obtain the maximum achievable information rate, but, in contrast to [1], we also derive the corresponding input signal distributions numerically and in closed form, respectively. Additionally, we show that the maximum achievable information rate depends on the ratio between the minimum required average and the maximum harvested instantaneous powers at the RX, and based on this observation, we propose a closed-form input distribution, which yields a suboptimal solution of the formulated optimization problem.
- Our simulation results reveal that RTD designs with improved reverse leakage current and breakdown voltage are preferable when the received signal power is low and high, respectively. Furthermore, we show that all derived input signal distributions yield practically identical achievable information rates and mutual informations between the TX and RX signals. Finally, we demonstrate the rate-power tradeoffs in THz SWIPT systems and show that for low and high received signal powers, this tradeoff is determined by the peak amplitude of the TX signal and the maximum instantaneous harvested power, respectively.

The rest of this paper is organized as follows. We present the adopted system model in Section II. In Section III, we propose a novel parametrized non-linear EH model for RTD-based RX designs. In Section IV, we derive input signal distributions for THz SWIPT. In Section V, we present numerical results. Finally, in Section V, we draw conclusions.

Throughout this paper, we use the following *notations*. We denote the sets of real, real non-negative, and non-negative integer numbers as \mathbb{R} , \mathbb{R}_+ , and \mathbb{N} , respectively. The real-part of a

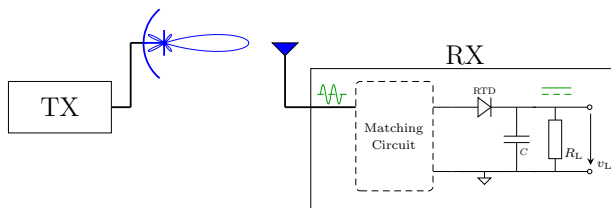


Fig. 1. THz SWIPT system model employing a TX with a highly directive antenna and a single-antenna RX equipped with an RTD-based rectifying circuit.

complex variable x is denoted by $\mathcal{R}\{x\}$, whereas $j = \sqrt{-1}$ is the imaginary unit. Functions $f_s(s)$ and $F_s(s)$ denote the probability density function (pdf) and cumulative density function (cdf) of random variable s , respectively. Furthermore, $f(x; y)$ denotes a function of variable x parametrized by y , $\delta(\cdot)$ is the Dirac delta function, and \triangleq means “is defined as”. $\mathbb{E}_s\{\cdot\}$ stands for statistical expectation with respect to random variable s . The domain and first-order derivative of one-dimensional function $g(\cdot)$ are denoted by $\mathcal{D}\{g\}$ and $g'(\cdot)$, respectively.

II. SYSTEM MODEL

We consider the SWIPT system shown in Fig. 1 where a TX equipped with a highly directive antenna sends a THz signal to a single-antenna RX. Since coherent demodulation of a THz-band received signal is challenging, the TX employs unipolar ASK modulation for SWIPT [22], [23]. Thus, the THz signal $r(t) \in \mathbb{R}$ received at the RX can be expressed as follows [20]:

$$r(t) = \sqrt{2}\mathcal{R}\{[hs(t) + n(t)] \exp(j2\pi f_c t)\}, \quad (1)$$

where h is the channel gain between TX and RX, which is assumed to be perfectly known at both devices, f_c is the carrier frequency, and $s(t) = \sum_k s[k]\phi(t - kT)$ and $n(t)$ are equivalent complex baseband (ECB) representations of the transmit signal and the additive white Gaussian noise (AWGN) at the RX antenna, respectively. Furthermore, here, $s[k] \in \mathbb{R}_+$, $k \in \mathbb{N}$, are independent and identically distributed (i.i.d.) realizations of a non-negative random variable s with pdf $f_s(s)$, $\phi(t)$ is a rectangular pulse that takes value 1, if $t \in [0, T)$, and 0, otherwise, and T is the duration of a symbol interval. To avoid signal distortion due to power amplifier non-linearities at the TX [14], [15], the maximum transmit signal power is bounded by A^2 . Thus, the support of f_s is confined to the interval $[0, A]$, i.e., $\mathcal{D}\{f_s\} \subseteq [0, A]$.

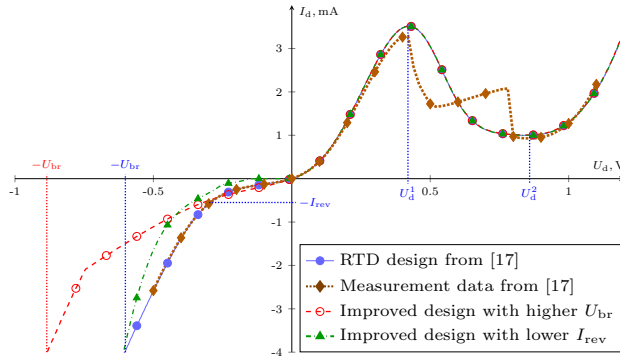


Fig. 2. I-V characteristic of the Keysight ADS RTD design in [16] matched to the measurement data in [16], and I-V characteristics of two improved RTD designs with higher breakdown voltage U_{br} and lower reverse leakage current I_{rev} , respectively.

III. EH MODELLING FOR RTD-BASED RXS

In this section, we present the RTD-based electrical EH circuit equipped at the RX and propose a general non-linear piecewise EH model to characterize the instantaneous output RX signal.

A. Electrical RX Circuit

Since Schottky diodes may not be efficient for THz signal demodulation and EH [18], we assume that the RX is equipped with an EH circuit comprising an antenna, a matching circuit, and an RTD-based rectifier with a load resistance R_L [9], [14], [15], as shown in Fig. 1. The matching circuit at the RX is a passive device that is designed to match the impedance of the antenna (typically, $50\ \Omega$ or $75\ \Omega$) to the input impedance of the rectifier [9], [14], [15], which is composed of the RTD, a low-pass filter with a capacitance C , and the load resistance R_L [19], [20].

Since EH circuits are envelope detectors [15], [19], we utilize the direct current (DC) voltage $v_L(t)$, $t \in [(k-1)T, kT)$, generated at the output of the RX circuit in time slot k , $k \in \mathbb{N}$, not only to charge the load, but also to decode information signal $s[k]$. Furthermore, as in [1] and [14], we neglect the ripples of the output voltage $v_L(t)$ across the resistance R_L and the dependence of $v_L(t)$ in time slot k , $k \in \mathbb{N}$, on information signals $s[p]$ transmitted prior to that time slot, $p < k$, $p \in \mathbb{N}$, caused by the non-ideality of the employed low-pass filter. Thus, we express the signal used for information decoding at the RX output, $y[k] \in \mathbb{R}$, in time slot k , $\forall k \in \mathbb{N}$, as

follows¹:

$$y[k] \triangleq \frac{v_L[k]}{\sqrt{R_L}} = \sqrt{\psi(|hs[k]|^2)} + n[k], \quad (2)$$

where $v_L[k]$, $n[k]$, and $\psi(\cdot)$ are the output voltage, equivalent output noise sample, and the function that maps the received signal power $\rho[k] = |hs[k]|^2$ to the power harvested at the load R_L in time slot $k, \forall k \in \mathbb{N}$, respectively. Function $\psi(\cdot)$, which models the RTD-based RX circuit in Fig. 1, will be derived in the next section. The output noise $n[k]$ in time slot $k, \forall k$, is composed of the received noise from external sources and the internal thermal noise generated by the components of the RX electrical circuit. In the following, for the derivation of the average harvested power at the RX, we assume that the impact of noise is negligible [9], [14], [15]. Furthermore, to characterize the performance of information decoding, we assume that the thermal noise originating from the RX components dominates, and thus, we neglect the dependency of $n[k]$ on the received power $\rho[k], \forall k$ [24]. Hence, we model the output noise samples $n[k], \forall k$, as i.i.d. realizations of AWGN with zero mean and variance σ^2 .

B. I-V characteristics of RTDs

In the following, we discuss the RTD employed at the THz RX in Fig. 1. We note that RTDs have multiple quantum barriers, and thus, the current flow I_d through the RTD is not a monotonically increasing function of the applied voltage U_d [16]. Instead, the corresponding I-V curve $I_d(U_d)$ may have multiple critical points, as shown in Fig. 2. For simplicity of presentation, we assume a triple-barrier RTD, whose corresponding I-V characteristic has a single region where the current flow I_d decreases when the applied voltage U_d increases, see Fig. 2 [16].

An ideal diode has a zero reverse current flow when the applied voltage is negative, i.e., for $U_d \in (-\infty, 0]$ [19]. However, due to the presence of minority charge carriers in the semiconductor, the reverse current of a realistic diode is negative, i.e., $I_d < 0$, even for small negative voltages $U_d < 0$ [19]. Moreover, if the voltage applied to an RTD is negative and smaller than the breakdown voltage, i.e., $U_d \leq -U_{br}$, the reverse current I_d grows large, as shown in Fig. 2, and may damage the RX [19].

¹In a practical RX design, one may use a DC voltage divider [20] to split the output DC current and utilize portions $\nu y[k]$ and $(1 - \nu)y[k]$ of the current flow $y[k], \forall k$, for EH and information decoding, respectively, where $\nu \in [0, 1]$ is the current splitting ratio. However, since the information rate does not depend on ν , we assume that the DC current $y[k]$ is directly utilized for decoding of the TX message.

Since the current flow of an RTD is determined by quantum processes and additionally depends on the signal frequency, determining the exact I-V characteristic of RTDs does not seem possible [16], [17]. Therefore, for our numerical results in Section V, we employ the compact Keysight ADS [21] numerical model of a triple-barrier RTD developed in [16], which was shown to fit the measured² I-V characteristic of the diode designed in [16], as shown in Fig. 2. Furthermore, since the rectifier performance depends on the negative-bias characteristics of the diode [20], to investigate the impact of the reverse leakage current and breakdown voltage of the RTD on SWIPT system performance, we also consider two improved RTD designs. In particular, by adjusting the parameters of the ADS diode model developed in [16], we design two improved RTDs, whose reverse current I_{rev} is lower and breakdown voltage U_{br} is higher compared to the RTD in [16], respectively. The I-V characteristics of the RTDs with improved I_{rev} and U_{br} are depicted by the green dash-dotted line and the red dashed line in Fig. 2, respectively.

C. Proposed EH Model

In contrast to Schottky diodes utilized for RF EH in [14], [15], the I-V characteristic of an RTD is not monotonic, as shown in Fig. 2. Therefore, the instantaneous harvested power $P_{\text{h}} = \frac{v_{\text{L}}^2}{R_{\text{L}}}$ of an RTD-based EH circuit may not be a monotonic non-decreasing function of the input power $\rho = |hs|^2$ [14], [16], [17]. Moreover, since a closed-form expression for the current flow I_{d} through an RTD is not available, the derivation of an accurate closed-form expression for the harvested power is not feasible [16], [17]. Therefore, as in [10], in the following, we propose a *general parametrized non-linear* EH model to characterize the instantaneous power harvested at the RX.

General Piecewise EH Model: We model the dependence of the harvested power on the received signal power ρ with the following continuous piecewise function $\psi(\rho)$ shown in Fig. 3:

$$\psi(\rho) = \begin{cases} \varphi_1(\rho), & \text{if } \rho \in [\rho_0, \rho_1), \\ \varphi_2(\rho), & \text{if } \rho \in [\rho_1, \rho_2), \\ \dots & \\ \varphi_N(\rho), & \text{if } \rho \in [\rho_{N-1}, \rho_{\max}], \end{cases} \quad (3)$$

²We note that the discrepancy between the I-V characteristic of the ADS RTD design in [16] and the measurement data in Fig. 2 is caused by non-idealities (parasitic oscillations) of the measurement setup used in [16].

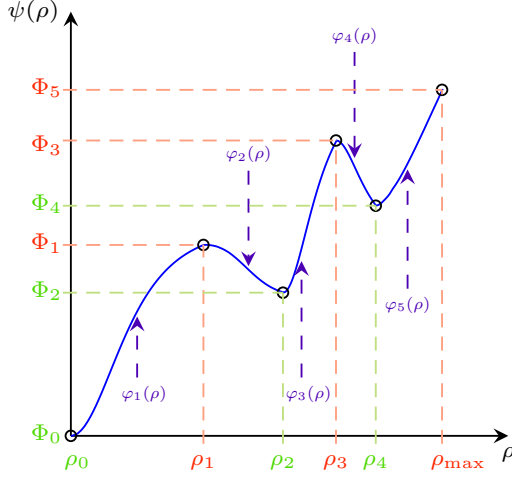


Fig. 3. Proposed EH model in (3) with $N = 5$ monotonic functions $\varphi_n(\cdot)$.

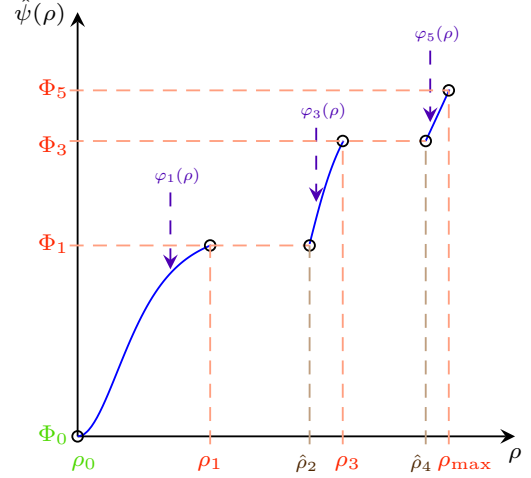


Fig. 4. Equivalent EH model for the solution of (8).

where function $\psi(\cdot)$ is defined in the domain $\mathcal{D}\{\psi\} = [\rho_0, \rho_{\max}]$ and ρ_{\max} is the maximum value of received signal power that does not drive the RTD into breakdown. Here, for modelling $\psi(\cdot)$, we need³ $N \in \mathbb{N}$ monotonic functions $\varphi_n(\cdot)$ with domains $\mathcal{D}\{\varphi_n\} = [\rho_{n-1}, \rho_n]$, $n \in \{1, 2, \dots, N-1\}$ and $\mathcal{D}\{\varphi_N\} = [\rho_{N-1}, \rho_{\max}]$, where $0 \triangleq \rho_0 \leq \rho_1 \leq \rho_2 \leq \dots \leq \rho_N \triangleq \rho_{\max}$. The number of functions N depends on the number of critical points in the I-V characteristic and the breakdown voltage U_{br} of the RTD. Furthermore, since the I-V characteristic of an RTD includes both regions where I_d increases when U_d grows and where I_d decreases when U_d grows, as shown in Fig. 2, we adopt parametrized monotonically increasing and decreasing functions $\varphi_n(\cdot)$ for odd and even values of n , i.e., $n \in \{1, 3, \dots\}$ and $n \in \{2, 4, \dots\}$ with $n \leq N$, respectively, as shown in Fig. 3. Finally, we express the average harvested power at the RX as function $\bar{P}_s(f_s)$ of the input pdf $f_s(\cdot)$, or equivalently, function $\bar{P}_x(f_x)$ of the pdf $f_x(\cdot)$ of signal $x = \sqrt{\psi(|h_s[k]|^2)}$ in (2) as follows:

$$\bar{P}_s(f_s) \triangleq \mathbb{E}_s\{\psi(|h_s|^2)\} = \mathbb{E}_x\{x^2\} \triangleq \bar{P}_x(f_x). \quad (4)$$

Here, we neglect the impact of noise since its contribution to the average harvested power is negligible [10], [14], [15].

³For the RX circuit shown in Fig. 1 with a single triple-barrier RTD, the number of functions required to model $\psi(\cdot)$ does not exceed $N = 3$ [17], [18]. However, for more complex RX designs with multiple RTDs, we may need $N > 3$ functions for accurate EH modelling.

Parametrized model of $\varphi_n(\cdot)$: Since an accurate analytical derivation of functions $\varphi_n(\cdot)$, $n \in \{1, 2, \dots, N\}$, is not feasible for an RTD-based EH circuit, we model $\varphi_n(\cdot)$, $\forall n$, by the following 5-parameter logistic function [25]:

$$\varphi_n(\rho) = B_n + (\Phi_{n-1} - B_n) \left[1 + \theta_n (\rho - \rho_{n-1})^{\alpha_n} \right]^{-\beta_n}. \quad (5)$$

Here, $B_n = \lim_{\rho \rightarrow \infty} \varphi_n(\rho)$ and $\Phi_n = \varphi_n(\rho_n)$, $\forall n$, with $\Phi_0 = 0$ and $\Phi_n \leq \Phi_{n+2}$, $\forall n \in \{0, 1, \dots, N-2\}$, as shown in Fig. 3. Parameters $\alpha_n, \beta_n, \theta_n \in \mathbb{R}_+$ in (5) characterize the non-linearity of $\varphi_n(\cdot)$, $\forall n$, and as in [10], can be obtained through a curve-fitting approach to optimize the agreement between $\psi(\cdot)$ and measurement or simulation data. Furthermore, as in [5]–[15], we assume that all parameters of the RX circuit are perfectly known at the TX.

IV. RATE-POWER TRADEOFF

In this section, we determine the optimal input distribution and characterize the rate-power tradeoff of the considered THz SWIPT system. To this end, we first formulate and solve an optimization problem for the maximization of the mutual information between the TX and RX signal subject to constraints on the average harvested power at the RX and the peak TX signal power. Next, since solving the optimization problem is computationally intensive for practical SWIPT systems, we obtain the input signal distribution maximizing the achievable information rate for a given required average harvested power at the RX. Finally, based on this result, we propose a closed-form TX signal distribution that also provides a suboptimal solution of the formulated optimization problem.

A. Problem Formulation and Optimal Solution

We characterize the performance of the THz SWIPT system by the tradeoff between the average harvested power at the RX $\bar{P}_s(f_s)$ in (4) and the mutual information $I_s(\cdot)$ between the TX and RX signals that can be expressed in nats per channel use as follows [14], [15], [26]:

$$I_s(f_s) = - \int_{-\infty}^{\infty} f_y(y; f_x) \ln f_y(y; f_x) dy - \frac{1}{2} \ln(2\pi e \sigma^2). \quad (6)$$

Here, $f_y(y; f_x)$ is the pdf of the RX output signal $y = x + n$ in (2) as a function of the pdf f_x of output information signal $x = \sqrt{\psi(|h_s[k]|^2)}$ and is given by [15], [26]:

$$f_y(y; f_x) = \int_{-\infty}^{\infty} f_x(x; f_s) f_n(y - x) dx, \quad (7)$$

where $f_x(x; f_s)$ is the pdf of the output information signal x for a given input pdf f_s and $f_n(n) = \frac{1}{\sqrt{2\pi\sigma^2}} \exp(-\frac{n^2}{2\sigma^2})$ is the pdf of the AWGN n .

To characterize the rate-power tradeoff, we determine the pdf f_s of transmit signal s that maximizes the mutual information $I_s(\cdot)$ for a given required average harvested power \bar{P}_{req} at the RX [4], [14], [15]. To this end, we formulate the following optimization problem:

$$\underset{f_s \in \mathcal{F}_s}{\text{maximize}} \quad I_s(f_s) \quad (8a)$$

$$\text{subject to} \quad \bar{P}_s(f_s) \geq \bar{P}_{\text{req}}, \quad (8b)$$

where $\mathcal{F}_s = \{f_s \mid \mathcal{D}\{f_s\} \subseteq [0, \bar{A}], \int_s f_s(s) ds = 1\}$ denotes the set of feasible input pdfs whose support does not exceed the maximum value $\bar{A} = \min\{A, \frac{\sqrt{\rho_{\text{max}}}}{|h|}\}$, such that the transmit signal amplitude is upper-bounded by A and the RTD is not driven into the breakdown.

To solve (8), in the following proposition, we first determine under which condition optimization problem (8) is feasible.

Proposition 1. *For a given $\bar{A} = \min\{A, \frac{\sqrt{\rho_{\text{max}}}}{|h|}\}$, optimization problem (8) is feasible if and only if $\bar{P}_{\text{req}} \in [0, \bar{P}_{\text{max}}]$ with $\bar{P}_{\text{max}} = \max_{\rho \in [0, |h\bar{A}|^2]} \psi(\rho)$.*

Proof. Please refer to Appendix A. ■

Proposition 1 highlights that for a given peak amplitude \bar{A} , the average power harvested at the RX is bounded by \bar{P}_{max} , and hence, a solution of (8) does not exist for $\bar{P}_{\text{req}} > \bar{P}_{\text{max}}$. Furthermore, we note that if $\bar{P}_{\text{req}} = \bar{P}_{\text{max}}$, the optimal pdf solving (8) is trivial and given by $f_s^{\text{opt}}(s) = \delta(s - \bar{A})$. In the following, we consider the case, where optimization problem (8) is feasible and the solution is not trivial, i.e., $\bar{P}_{\text{req}} \in [0, \bar{P}_{\text{max}})$.

We note that since function $\psi(\cdot)$ is, in general, not invertible, the mapping between the input pdf f_s and the pdf f_x , and hence, mutual information $I_s(\cdot)$ in (6) may not be unique. Therefore, in the following proposition, we show that to determine an optimal input pdf f_s^{opt} as solution of (8), the proposed general piecewise EH model in (3) can be replaced by an equivalent EH model that is increasing in its domain.

Proposition 2. *There exists an optimal input pdf solving (8) that satisfies $f_s^{\text{opt}}(s) = 0, \forall s \in \mathcal{S}$, where $\mathcal{S} = (s_1, \hat{s}_2] \cup (s_3, \hat{s}_4] \cup \dots \cup (s_{\hat{N}-1}, \hat{s}_{\hat{N}}]$. Here, $s_n = \sqrt{\frac{\rho_n}{|h|^2}}$ and $\hat{s}_n = \sqrt{\frac{\hat{\rho}_n}{|h|^2}}, n \in \{1, 3, 5, \dots, \hat{N}\}$. Furthermore, $\hat{\rho}_n = \varphi_{n+1}^{-1}(\varphi_{n-1}(\rho_{n-1}))$, $n \in \{2, 4, 6, \dots, \hat{N} - 1\}$, and $\hat{N} \in \mathbb{N}$ is the maximum number $n \leq N$ such that $\hat{\rho}_{n-1}$ exists.*

Proof. Please refer to Appendix B. ■

Proposition 2 reveals that the solution of problem (8) may not be unique and there exists an optimal input pdf with $f_s^{\text{opt}} = 0, \forall s \in \mathcal{S}$. Thus, for any given pdf f_x , an input pdf f_s that yields f_x can be obtained as $f_s(s) = \frac{\partial}{\partial s} F_x(\hat{\psi}(|hs|^2))$, where $F_x(x) = \int_0^x f_x(\tilde{x}) d\tilde{x}$ is the corresponding cdf of x . Here, $\hat{\psi}(\cdot)$ is the equivalent EH model with $\hat{\psi}(\rho) = \psi(\rho), \forall \rho \in \mathcal{D}\{\hat{\psi}\}$, that is shown in Fig. 4. The domain of function $\hat{\psi}(\cdot)$ is $\mathcal{D}\{\hat{\psi}\} = [\rho_0, \rho_1) \cup [\hat{\rho}_2, \rho_3) \cup [\hat{\rho}_4, \rho_5) \cup \dots \cup [\hat{\rho}_{\hat{N}-1}, \rho_{\max}]$. We note that in contrast to EH model $\psi(\cdot)$ in (3), function $\hat{\psi}(\cdot)$ is monotonically increasing in its domain $\mathcal{D}\{\hat{\psi}\}$, and thus, is invertible. Therefore, for a given f_x , the input pdf f_s exists and is unique.

To obtain an optimal pdf f_s^{opt} as solution of (8), we can first determine the optimal pdf f_x^{opt} of the signal x that solves the following equivalent optimization problem:

$$\underset{f_x \in \mathcal{F}_x}{\text{maximize}} \quad I_x(f_x) \quad (9a)$$

$$\text{subject to} \quad \bar{P}_x(f_x) \geq \bar{P}_{\text{req}}, \quad (9b)$$

where $I_x(f_x) = -\int_{-\infty}^{\infty} f_y(y; f_x) \ln f_y(y; f_x) dy - \frac{1}{2} \ln(2\pi e\sigma^2)$ is the mutual information between signals x and y expressed as a function of f_x , i.e., we have $I_x(f_x) = I_s(f_s)$ in (6) if input pdf f_s yields f_x . Here, $\mathcal{F}_x = \{f_x \mid \mathcal{D}\{f_x\} \subseteq [0, \sqrt{\bar{P}_{\text{max}}}], \int_x f_x(x) dx = 1\}$ denotes the feasible set of pdfs f_x that correspond to the input pdfs $f_s \in \mathcal{F}_s$ in (8).

We note that determining the optimal pdf f_x^{opt} as solution of (9) may not be possible in closed form. However, optimization problem (9) is convex, and hence, we can solve (9) numerically by discretizing feasible set \mathcal{F}_x [27]. To this end, we define a uniform constellation set $\mathcal{X} = \{x_0, x_1, \dots, x_{K-1}\}$ of size $K \in \mathbb{N}$, where $x_k = \frac{k}{K-1} \sqrt{\bar{P}_{\text{max}}}$. Next, for $\mathcal{F}_x = \mathcal{X}$, we determine the discrete pdf f_x^{opt} as solution of (9) utilizing CVX [14], [15], [28]. For the obtained pdf f_x^{opt} , we find the corresponding input pdf $f_s^{\text{opt}}(s) = \frac{\partial}{\partial s} F_x^{\text{opt}}(\hat{\psi}(|hs|^2))$, where $F_x^{\text{opt}}(x) = \int_0^x f_x^{\text{opt}}(\tilde{x}) d\tilde{x}$ is the corresponding cdf of x .

The algorithm for determining the input pdf f_s^{opt} solving (8) is summarized in **Algorithm 1**. We note that as $K \rightarrow \infty$, the obtained discrete pdf f_s^{opt} converges to the optimal solution of (8) [14]. Furthermore, the computational complexity and the accuracy of the obtained solution grow polynomially with constellation size K [29]. Thus, an accurate solution of (8) requires a high computational complexity, which may not be feasible in practical THz SWIPT systems, where the required data rates are high and channel time coherence intervals are small [2], [3].

Algorithm 1: Algorithm for determining the input pdf f_s^{opt} .

Initialize: Peak signal amplitude \bar{A} , required average harvested power \bar{P}_{req} , EH model $\psi(\cdot)$, channel coefficient h , size of the constellation set K .

1. Find $\bar{P}_{\text{max}} = \max_{\rho \in [0, |h\bar{A}|^2]} \hat{\psi}(\rho)$.

2. Discretize the feasible set $\mathcal{F}_x = \{x_0, x_1, \dots, x_{K-1}\}$, where $x_k = \frac{k}{K-1} \sqrt{\bar{P}_{\text{max}}}$, $\forall k$

3. Determine the optimal pdf $f_x^{\text{opt}} \in \mathcal{F}_x$ as solution of (9) and find the corresponding cdf F_x^{opt} and pdf f_s^{opt}

Output: Optimal input pdf f_s^{opt}

Therefore, in the following, as a suboptimal solution of (8), we derive an input signal distribution that maximizes the achievable information rate between the TX and RX signals.

B. Achievable Rate-Power Tradeoff

Since accurately determining an optimal input pdf f_s^{opt} that solves (8) is challenging for THz SWIPT systems, in the following, for a given \bar{A} and $\bar{P}_{\text{req}} \in [0, \bar{P}_{\text{max}})$, we obtain a low-complexity suboptimal solution of (8). To this end, in the following lemma, we first derive a lower bound on the maximum mutual information in (9).

Lemma 1. For any values of \bar{A} and $\bar{P}_{\text{req}} \in [0, \bar{P}_{\text{max}}]$, the maximum mutual information as solution of (9) is lower-bounded by

$$I_x(f_x^{\text{opt}}) = \max_{f_x \in \bar{\mathcal{F}}_x} I_x(f_x) \geq \max_{f_x \in \bar{\mathcal{F}}_x} J_x(f_x) \triangleq J_{\bar{\mathcal{F}}_x}^*, \quad (10)$$

where $\bar{\mathcal{F}}_x = \{f_x \mid f_x \in \mathcal{F}_x, \bar{P}_x(f_x) \geq \bar{P}_{\text{req}}\}$ is the feasible set of problem (9). Furthermore, $J_x(f_x) = \frac{1}{2} \ln \left(1 + \frac{e^{2h_x(f_x)}}{2\pi e \sigma^2} \right)$ is the achievable information rate as function of $f_x(\cdot)$ and $h_x(f_x) = - \int f_x(x) \ln f(x) dx$ is the entropy of random variable x for a given pdf $f_x(\cdot)$.

Proof. Please refer to Appendix C. ■

Lemma 1 shows that the maximum mutual information $I_x(f_x^{\text{opt}})$ as solution of (9) can be lower-bounded by the maximum achievable information rate $J_{\bar{\mathcal{F}}_x}^*$, which, in turn, is obtained as a solution of the optimization problem in (10). In the following, as a suboptimal solution of (9), for given \bar{A} and $\bar{P}_{\text{req}} \in [0, \bar{P}_{\text{max}})$, we determine the pdfs f_x^{ach} and f_s^{ach} of random variables x and s , respectively, that yield the maximum achievable rate $J_{\bar{\mathcal{F}}_x}^*$. First, in the following proposition, we show that for small required average harvested powers \bar{P}_{req} , constraint (9b) in the definition of $\bar{\mathcal{F}}_x$ can be relaxed and the pdf f_x^{ach} can be obtained in closed form.

Proposition 3. For a given $\bar{A} = \min\{A, \frac{\sqrt{\rho_{\max}}}{|h|}\}$ and required average harvested powers satisfying $\bar{P}_{\text{req}} \in [0, \frac{1}{3}\bar{P}_{\max}]$, the maximum achievable information rate is given by $J_{\bar{\mathcal{F}}_x}^* = \frac{1}{2} \ln\left(1 + \frac{\bar{P}_{\max}}{2\pi e\sigma^2}\right)$ and the corresponding pdf of x is

$$f_x^{\text{ach}}(x) = \frac{1}{\sqrt{\bar{P}_{\max}}}, \quad x \in [0, \sqrt{\bar{P}_{\max}}]. \quad (11)$$

Proof. Please refer to Appendix D. ■

Proposition 3 reveals that if the required average harvested power \bar{P}_{req} is low, there is no tradeoff between the achievable information rate and the average harvested power and the corresponding $J_{\bar{\mathcal{F}}_x}^*$, f_x^{ach} , and thus, f_y^{ach} can be computed in closed form. In the following, we derive the output pdf f_y^{ach} in (7) when the pdf of x is given by (11).

Corollary 1. If random variable x has pdf f_x^{ach} in (11), the output pdf in (7) is given by

$$f_y^{\text{ach}}(y; f_x^{\text{ach}}) = \frac{1}{\sqrt{\bar{P}_{\max}}} \left[Q\left(\frac{y - \sqrt{\bar{P}_{\max}}}{\sigma}\right) - Q\left(\frac{y}{\sigma}\right) \right]. \quad (12)$$

Proof. Please refer to Appendix E. ■

In the next proposition, we consider the case where $\bar{P}_{\text{req}} \in [\frac{1}{3}\bar{P}_{\max}, \bar{P}_{\max})$ and characterize the corresponding maximum achievable information rate $J_{\bar{\mathcal{F}}_x}^*$ and f_x^{ach} .

Proposition 4. For a given $\bar{A} = \min\{A, \frac{\sqrt{\rho_{\max}}}{|h|}\}$ and a required average harvested power $\bar{P}_{\text{req}} \in [\frac{1}{3}\bar{P}_{\max}, \bar{P}_{\max})$, the maximum achievable information rate $J_{\bar{\mathcal{F}}_x}^*$ in (10) is given by

$$J_{\bar{\mathcal{F}}_x}^* = \frac{1}{2} \ln\left(1 + \frac{e^{2\mu_0 - 2\mu_1^2 \frac{\bar{P}_{\text{req}}}{\bar{P}_{\max}}}}{2\pi e\sigma^2}\right). \quad (13)$$

Furthermore, the corresponding pdf of x that solves (9) can be expressed as

$$f_x^{\text{ach}}(x) = \exp\left(-\mu_0 + \mu_1^2 \frac{x^2}{\bar{P}_{\max}}\right), \quad x \in [0, \sqrt{\bar{P}_{\max}}], \quad (14)$$

where $\mu_0 = \mu_1^2 + \ln\left(\frac{\sqrt{\bar{P}_{\max}}}{1 + 2\mu_1^2 \frac{\bar{P}_{\text{req}}}{\bar{P}_{\max}}}\right)$. Here, $\mu_1 \in \mathbb{R}_+$ is the solution of the following equation:

$$\frac{\bar{P}_{\text{req}}}{\bar{P}_{\max}} = \frac{\exp(\mu_1^2)}{\sqrt{\pi}\mu_1 \text{Ei}(\mu_1)} - \frac{1}{2\mu_1^2} \quad (15)$$

with imaginary error function $\text{Ei}(\cdot)$.

Proof. Please refer to Appendix F. ■

Proposition 4 shows that if $\bar{P}_{\text{req}} \in [\frac{1}{3}\bar{P}_{\max}, \bar{P}_{\max})$, there is a tradeoff between the maximum achievable information rate and the average harvested power. Furthermore, for given \bar{A} and \bar{P}_{req} ,

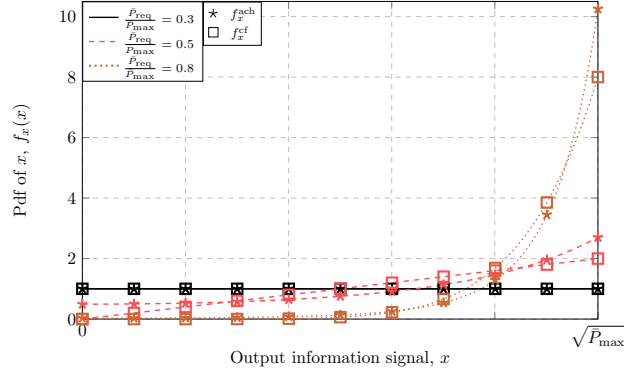


Fig. 5. The pdfs f_x^{ach} of x in (11) and (14) and proposed closed-form pdfs $f_x^{\text{cf}}(x)$ in (17) for different power ratios $\frac{\bar{P}_{\text{req}}}{\bar{P}_{\text{max}}}$.

the pdf f_x^{ach} and the maximum achievable information rate $J_{\mathcal{F}_x}^*$ depend on the power ratio $\frac{\bar{P}_{\text{req}}}{\bar{P}_{\text{max}}}$ in (15). The pdfs f_x^{ach} obtained for different power ratios $\frac{\bar{P}_{\text{req}}}{\bar{P}_{\text{max}}}$ are shown in Fig. 5. In the following corollary, we provide the output pdf of y in (7) when the signal x follows the pdf in (14).

Corollary 2. *If random variable x follows the distribution with pdf f_x^{ach} in (14), the output pdf f_y^{ach} can be expressed as follows:*

$$f_y^{\text{ach}}(y; f_x^{\text{ach}}) = \frac{1}{\mu_4} \exp\left(\frac{y^2}{\bar{P}_{\text{max}}} \frac{\mu_1^2}{\mu_4^2} - \mu_0\right) \left[Q\left(\frac{y - \mu_4^2 \sqrt{\bar{P}_{\text{max}}}}{\mu_4 \sigma}\right) - Q\left(\frac{y}{\mu_4 \sigma}\right) \right] \quad (16)$$

with $\mu_4 = \sqrt{1 - 2 \frac{\mu_1^2}{\bar{P}_{\text{max}}} \sigma^2}$.

Proof. Please refer to Appendix G. ■

We note that if $\bar{P}_{\text{req}} \in [\frac{1}{3}\bar{P}_{\text{max}}, \bar{P}_{\text{max}})$, the maximum information rate $J_{\mathcal{F}_x}^*$, the pdf f_x^{ach} , and hence, f_s^{ach} and mutual information $I_s(f_s^{\text{ach}})$ require μ_1 as solution of (15), which, in general, can not be obtained in closed form. Therefore, in the following, we propose an iterative algorithm based on bisection to determine the input pdf f_s^{ach} maximizing the achievable information rate in (10). To this end, we first note that function $g(\mu_1) = \frac{\exp(\mu_1^2)}{\sqrt{\pi\mu_1}\text{Ei}(\mu_1)} - \frac{1}{2\mu_1^2}$ is monotonically increasing⁴ in its domain $\mathcal{D}\{g\} = \mathbb{R}_+$ and $g(\mu_1) \in [\frac{1}{3}, 1)$. Next, we find a lower and an upper bound, $\mu_{1\text{lo}}$ and $\mu_{1\text{up}}$, of the initial interval for the bisection algorithm, such that $g(\mu_{1\text{lo}}) \leq \frac{\bar{P}_{\text{req}}}{\bar{P}_{\text{max}}}$ and $g(\mu_{1\text{up}}) \geq \frac{\bar{P}_{\text{req}}}{\bar{P}_{\text{max}}}$. To this end, we create a lookup table comprising an array $\mathcal{M} = \{\mu^1, \mu^2, \dots, \mu^{N_{\mathcal{M}}}\} \in \mathbb{R}_+^{N_{\mathcal{M}}}$, where

⁴The monotonicity of $g(\cdot)$ can be verified by examining the first-order derivative $g'(\mu) = \frac{1}{\mu^3} + \frac{2\exp(\mu^2)}{\sqrt{\pi}\text{Ei}(\mu)} \left[1 - \frac{1}{2\mu^2} - \frac{\exp(\mu^2)}{\sqrt{\pi}\mu\text{Ei}(\mu)}\right] \geq 0, \forall \mu \in \mathbb{R}_+$.

Algorithm 2: Algorithm for determining the input pdf f_s^{ach} .

Initialize: Peak amplitude \bar{A} , required average harvested power \bar{P}_{req} , EH model $\psi(\cdot)$, channel coefficient h , lookup table arrays \mathcal{M} and \mathcal{G} , and accuracy ϵ .

1. Find $\bar{P}_{\text{max}} = \max_{\rho \in [0, |h\bar{A}|^2]} \hat{\psi}(\rho)$

if $\bar{P}_{\text{req}} \in [0, \frac{1}{3}\bar{P}_{\text{max}}]$ **then**

2. Determine the pdf $f_x^{\text{ach}}(x) = \frac{1}{\sqrt{\bar{P}_{\text{max}}}}$ with $x \in [0, \sqrt{\bar{P}_{\text{max}}}]$

else

3. Identify $n_{\text{up}} = \min\{n \mid g^n \geq \frac{\bar{P}_{\text{req}}}{\bar{P}_{\text{max}}}\}$, where $g^n \in \mathcal{G}, \forall n$, and set $\mu_{\text{up}} = \mu^{n_{\text{up}}} \in \mathcal{M}$ and

$$\mu_{\text{lo}} = \mu^{n_{\text{up}}-1} \in \mathcal{M}$$

4. Utilize the bisection approach to find μ_1 :

while $|\mu_{\text{up}} - \mu_{\text{lo}}| > \epsilon$ **do**

4.1. Find $\mu^c = \frac{\mu_{\text{up}} + \mu_{\text{lo}}}{2}$

4.2. Set $\mu_{\text{up}} = \mu^c$ if $g(\mu^c) > \frac{\bar{P}_{\text{req}}}{\bar{P}_{\text{max}}}$ and $\mu_{\text{lo}} = \mu^c$, otherwise

end

5. Set $\mu_1 = \frac{\mu_{\text{up}} + \mu_{\text{lo}}}{2}$

6. Determine the pdf $f_x^{\text{ach}}(x) = \exp(-\mu_0 + \mu_1^2 \frac{x^2}{\bar{P}_{\text{max}}})$, where $x \in [0, \sqrt{\bar{P}_{\text{max}}}]$ and $\mu_0 \in \mathbb{R}_+$ is given in

Proposition 4

8. Find the cdf $F_x^{\text{ach}}(x) = \int_0^x f_x^{\text{ach}}(\tilde{x})d\tilde{x}$ and input pdf $f_s^{\text{ach}}(s) = \frac{\partial}{\partial s} F_x^{\text{ach}}(\hat{\psi}(|hs|^2))$

Output: The input pdf f_s^{ach} .

$\mu^1 = 0$ and $\mu^i > \mu^j, \forall i > j$, of size $N_{\mathcal{M}}$ and a corresponding array $\mathcal{G} = \{g^1, g^2, \dots, g^{N_{\mathcal{M}}}\}$ with $g^n = g(\mu^n), n \in \{1, 2, \dots, N_{\mathcal{M}}\}$. We identify⁵ the array index $n_{\text{up}} = \min\{n \mid g^n \geq \frac{\bar{P}_{\text{req}}}{\bar{P}_{\text{max}}}\}$ and set $\mu_{\text{up}} = \mu^{n_{\text{up}}}$ and $\mu_{\text{lo}} = \mu^{n_{\text{up}}-1}$.

Then, we utilize the bisection algorithm to find the parameter μ_1 in the interval $[\mu_{\text{lo}}, \mu_{\text{up}}]$ that yields $g(\mu_1) = \frac{\bar{P}_{\text{req}}}{\bar{P}_{\text{max}}}$. In particular, in iteration $p \geq 1$, we calculate the mid point of the interval, $\mu^c = \frac{\mu_{\text{lo}} + \mu_{\text{up}}}{2}$. We compare the value of function $g(\cdot)$ in the mid point with the power ratio $\frac{\bar{P}_{\text{req}}}{\bar{P}_{\text{max}}}$ and we set $\mu_{\text{up}} = \mu^c$ if $g(\mu^c) > \frac{\bar{P}_{\text{req}}}{\bar{P}_{\text{max}}}$ and $\mu_{\text{lo}} = \mu^c$, otherwise. Finally, if $|\mu_{\text{up}} - \mu_{\text{lo}}| \leq \epsilon$, where ϵ is a predefined desired accuracy, we set $\mu_1 = \frac{\mu_{\text{up}} + \mu_{\text{lo}}}{2}$ and stop the bisection search. With the determined parameter μ_1 , we find μ_0 and f_x^{ach} in Proposition 4. The corresponding input pdf is given by $f_s^{\text{ach}}(s) = \frac{\partial}{\partial s} F_x^{\text{ach}}(\hat{\psi}(|hs|^2))$, where $F_x^{\text{ach}}(x) = \int_0^x f_x^{\text{ach}}(\tilde{x})d\tilde{x}$ is the cdf of x . Similar to f_s^{opt} , pdf f_s^{ach} exists and is unique due to the monotonicity of the equivalent EH model $\hat{\psi}(\cdot)$.

The proposed iterative algorithm for determining the input pdf f_s^{ach} as a suboptimal solution of

⁵We note that $g(\mu) \rightarrow 1$ when $\mu \rightarrow \infty$. Therefore, if such $n_{\text{up}} \in \{1, 2, \dots, N_{\mathcal{M}}\}$ does not exist, we obtain the pdf of x as $f_x^{\text{ach}} = \delta(x - \sqrt{\bar{P}_{\text{max}}})$.

(8) is summarized in **Algorithm 2**. We note that for $\bar{P}_{\text{req}} \in [0, \frac{1}{3}\bar{P}_{\text{max}}]$, the input pdf f_s^{ach} can be obtained in closed form. However, if $\bar{P}_{\text{req}} \in (\frac{1}{3}\bar{P}_{\text{max}}, \bar{P}_{\text{max}})$, the proposed algorithm still requires a numerical solution of (15), which may not be desirable in practice. Therefore, based on the obtained pdf f_x^{ach} maximizing the achievable information rate, in the following, we propose a closed-form suboptimal pdf f_x^{cf} as a suboptimal solution of (9).

C. Proposed Closed-form Input Distribution

We note that when the required average harvested power is low, i.e., $\bar{P}_{\text{req}} \leq \frac{1}{3}\bar{P}_{\text{max}}$, the pdf $f_x^{\text{ach}} \in \bar{\mathcal{F}}_x$ maximizing the achievable information rate in (10) is uniform and given by (11). Furthermore, for high required average harvested powers satisfying $\bar{P}_{\text{req}} \in (\frac{1}{3}\bar{P}_{\text{max}}, \bar{P}_{\text{max}})$, the pdf $f_x^{\text{ach}}(x)$ in (14) is a monotonic increasing function of $x \in [0, \sqrt{\bar{P}_{\text{max}}}]$. Finally, if $\bar{P}_{\text{req}} = \bar{P}_{\text{max}}$, the optimal pdf solving (9) is trivial and is given by $f_x^{\text{opt}}(x) = \delta(x - \sqrt{\bar{P}_{\text{max}}})$. Motivated by these observations, we propose to employ the following closed-form suboptimal pdf f_x^{cf} of x , which is uniform, monotonically increasing, and a singleton function for $\bar{P}_{\text{req}} \leq \frac{1}{3}\bar{P}_{\text{max}}$, $\bar{P}_{\text{max}} < \bar{P}_{\text{req}} < \frac{1}{3}\bar{P}_{\text{max}}$, and $\bar{P}_{\text{req}} = \bar{P}_{\text{max}}$, respectively:

$$f_x^{\text{cf}}(x) = \alpha P_{\text{max}}^{-\frac{\alpha}{2}} x^{\alpha-1}, \quad x \in [0, \sqrt{\bar{P}_{\text{max}}}] \quad (17)$$

We note that f_x^{cf} is the pdf of the scaled Beta distribution (or, equivalently, Kumaraswamy distribution) with parameters α and 1 [30]. It can be shown that for any $\alpha > 0$, pdf f_x^{cf} with $\mathcal{D}\{f_x^{\text{cf}}\} = [0, \sqrt{\bar{P}_{\text{max}}}]$ is valid, i.e., we have $\int f_x^{\text{cf}}(x)dx = 1$. Furthermore, the proposed pdf $f_x^{\text{cf}} \in \bar{\mathcal{F}}_x$, i.e., f_x^{cf} satisfies constraint (9b), if and only if $\alpha \geq \alpha_{\bar{\mathcal{F}}_x} \triangleq \frac{2\bar{P}_{\text{req}}}{\bar{P}_{\text{max}} - \bar{P}_{\text{req}}}$. Moreover, if $\frac{\bar{P}_{\text{req}}}{\bar{P}_{\text{max}}} = \frac{1}{3}$, we have $\alpha = \alpha_{\bar{\mathcal{F}}_x} = 1$, and similar to f_x^{ach} in (11), pdf $f_x^{\text{cf}}(x) = P_{\text{max}}^{-\frac{1}{2}}$ is uniform. Thus, we set parameter $\alpha = \max\{\alpha_{\bar{\mathcal{F}}_x}, 1\}$. The proposed pdf f_x^{cf} is shown in Fig. 5 for different power ratios $\frac{\bar{P}_{\text{req}}}{\bar{P}_{\text{max}}}$. Finally, we obtain the corresponding transmit signal pdf f_s^{cf} in closed form as $f_s^{\text{cf}}(s) = \frac{\partial}{\partial s} F_x^{\text{cf}}(\hat{\psi}(|hs|^2))$, where $F_x^{\text{cf}}(x) = \int_0^x f_x^{\text{cf}}(\tilde{x})d\tilde{x}$ is the cdf of x .

In the following proposition, we derive the achievable information rate $J_x(\cdot)$ in (10) when the pdf of x is given by (17).

Proposition 5. *If random variable x follows pdf f_x^{cf} in (17), the achievable mutual information in (10) is given by*

$$J_x(f_x^{\text{cf}}) = \frac{1}{2} \ln \left(1 + \frac{\bar{P}_{\text{max}} e^{2\frac{\alpha-1}{\alpha}}}{2\pi e \sigma^2 \alpha^2} \right), \quad (18)$$

Proof. Please refer to Appendix H. ■

Proposition 5 reveals that for $\alpha = 1$, i.e., for $\bar{P}_{\text{req}} \leq \frac{1}{3}\bar{P}_{\text{max}}$, the pdf f_x^{cf} in (17) yields the maximum achievable information rate $J_x(f_x^{\text{cf}}) = J_{\mathcal{F}_x}^*$ in Proposition 3. However, if $\bar{P}_{\text{req}} \in (\frac{1}{3}\bar{P}_{\text{max}}, \bar{P}_{\text{max}})$, the achievable information rate in (18) may be lower than the maximum value in (13), i.e., we have $J_x(f_x^{\text{cf}}) \leq J_{\mathcal{F}_x}^*$. In the next section, we numerically evaluate the performance of THz SWIPT systems and show that all obtained input pdfs, i.e., f_s^{opt} , f_s^{ach} , and f_s^{cf} , yield practically identical mutual information $I_s(\cdot)$ for all considered values of A and \bar{P}_{req} .

V. NUMERICAL RESULTS

In this section, we evaluate the performance of the considered THz SWIPT system via numerical simulations. To this end, we first specify the parameters of the adopted simulation setup and tune the parameters of the proposed parametrized EH model to match circuit simulation results. Next, we evaluate the mutual information and achievable information rate of the THz SWIPT system when the derived input signal distributions are adopted at the TX. Finally, we study the tradeoff between the mutual information and average harvested power at the RX.

A. Simulation Setup

For our numerical simulations, we assume a LoS between the TX and RX and model the channel as $h = \tilde{h}\hat{h}$, where $\tilde{h} = \frac{c_l}{4\pi d f_c} \sqrt{G_T G_R}$ and \hat{h} are the large- and small-scale channel coefficients, respectively. Here, $G_T = G_R = 100$, c_l , $f_c = 300$ GHz, and $d = 0.1$ m are the TX and RX antenna gains, speed of light, carrier frequency⁶, and distance between the TX and RX, respectively. Unless specified otherwise, we model the small-scale fading coefficient \hat{h} as a Rician distributed random variable with Rician factor 1 [15]. In Algorithm 1, we set the size of the constellation set $K = 1000$, while the accuracy and the lookup table arrays in Algorithm 2 are set to $\epsilon = 10^{-3}$ and $\mathcal{M} = \{0, 10^{-1}, 10^0, 10^1, 10^2, 10^3, 10^4\}$ and $\mathcal{G} = \{\tilde{g} \mid \tilde{g} = g(\mu), \forall \mu \in \mathcal{M}\}$, respectively. The noise variance at the output of the RX is set to $\sigma^2 = -50$ dBm. We average all simulation results over 1000 channel realizations.

B. RX Circuit Simulations and EH Model Fitting

First, we tune the parameters of the proposed general EH model $\psi(\cdot)$ to match the circuit simulation results. To this end, we model the RTD-based EH circuit shown in Fig. 1 with circuit

⁶For our simulations, we utilize $f_c = 300$ GHz since the I-V characteristics of the Keysight ADS [21] RTD design from [16] are shown to accurately match the measurements results in [16] for sub-THz frequencies.

TABLE I
TUNED PARAMETERS OF THE EH MODEL IN (3).

RTD design in [16]		RTD design with improved I_{rev}		RTD design with improved U_{br}		
$\rho_1 = 1.8 \text{ mW}, \rho_2 = 2.4 \text{ mW}$		$\rho_1 = 2.1 \text{ mW}, \rho_2 = 3 \text{ mW}$		$\rho_1 = 4.1 \text{ mW}, \rho_2 = 4.17 \text{ mW}, \rho_3 = 6.18 \text{ mW}$		
$\varphi_1(\cdot)$	$\varphi_2(\cdot)$	$\varphi_1(\cdot)$	$\varphi_2(\cdot)$	$\varphi_1(\cdot)$	$\varphi_2(\cdot)$	$\varphi_3(\cdot)$
$B_1 = 71.6 \mu\text{W}$	$B_2 = 25 \mu\text{W}$	$B_1 = 315 \mu\text{W}$	$B_2 = 104 \mu\text{W}$	$B_1 = 3.6 \text{ mW}$	$B_2 = 535 \mu\text{W}$	$B_3 = 2.85 \text{ mW}$
$\alpha_1 = 1.432$	$\alpha_2 = 1.841$	$\alpha_1 = 1.46$	$\alpha_2 = 2.601$	$\alpha_1 = 1.534$	$\alpha_2 = 3.492$	$\alpha_3 = 1.492$
$\beta_1 = 0.778$	$\beta_2 = 0.445$	$\beta_1 = 0.527$	$\beta_2 = 0.703$	$\beta_1 = 0.289$	$\beta_2 = 10^4$	$\beta_3 = 0.244$
$\theta_1 = 2174.9$	$\theta_2 = 956.8$	$\theta_1 = 3580$	$\theta_2 = 1100$	$\theta_1 = 241.6$	$\theta_2 = 1692$	$\theta_3 = 294.8$

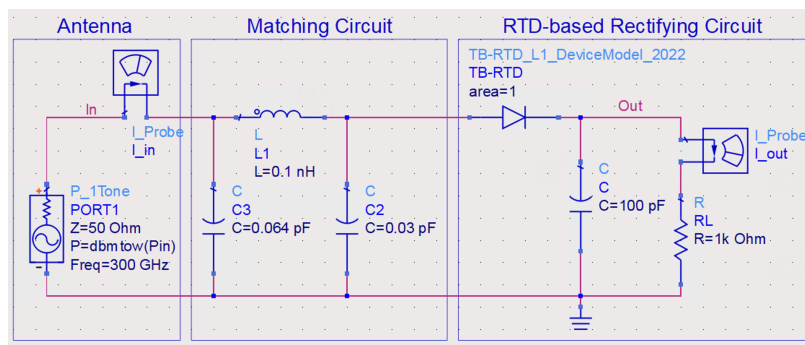


Fig. 6. Circuit simulation setup in Keysight ADS [21].

parameters $C = 100 \text{ pF}$ and $R_L = 1 \text{ k}\Omega$ [14] using the harmonic balance Keysight ADS [21] circuit simulations, as shown in Fig. 6. In particular, we assume an antenna impedance of 50Ω , and for each considered input power ρ , we design the matching circuit to achieve near-perfect impedance matching between the antenna and the rectifier of the EH circuit, see Fig. 6 [14], [15]. To investigate the impact of the breakdown voltage and leakage current of the RTD on the performance of THz SWIPT systems, in our simulations, we consider not only the Keysight ADS [21] design of the triple-barrier RTD proposed in [16], but also two improved RTD designs. In particular, we adopt RTD designs with lower reverse leakage current I_{rev} and higher breakdown voltage U_{br} compared to the design in [16], respectively, whose I-V characteristics are shown in Fig. 2. For all considered RTDs, the proposed EH model $\psi(\cdot)$ tuned to match the circuit simulation results and obtained by Keysight ADS is shown in Fig. 7 and the corresponding model parameters are summarized in Table I.

We observe in Fig. 7 that for all considered RTDs, as expected, the instantaneous harvested power grows with the input signal power for $\rho \in [0, \rho_1)$. Then, for the RTD design in [16] and

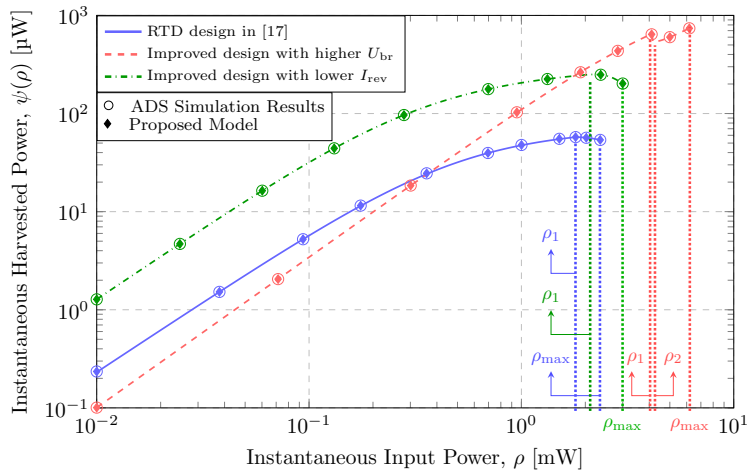


Fig. 7. Proposed EH model tuned to match the circuit simulation results.

the RTD with improved I_{rev} , the power harvested at the EH receiver decreases with the input power in the interval $[\rho_1, \rho_{\text{max}}]$ until the maximum power level $\rho = \rho_{\text{max}}$ is reached. Since the maximum power level ρ_{max} depends not only on the breakdown voltage U_{br} , but also on the reverse-bias current flow I_{d} for $U_{\text{d}} \in (-U_{\text{br}}, 0)$, the values of ρ_{max} for both diodes are similar but not identical [19]. Furthermore, since for both RTD designs, the breakdown voltage U_{br} is low, functions $\varphi_1(\cdot)$ and $\varphi_2(\cdot)$ are sufficient for EH modelling, and thus, we have $\rho_2 = \rho_{\text{max}}$. On the contrary, we observe in Fig. 7 that for the RTD with the higher breakdown voltage U_{br} , similar to Fig. 3, the harvested power at the EH receiver decreases in $\rho \in [\rho_1, \rho_2]$ and increases in $\rho \in [\rho_2, \rho_{\text{max}}]$. In other words, the corresponding EH circuit can operate at a higher power level compared to the EH circuit equipped with the RTD in [16]. Therefore, for modelling the corresponding EH circuit, not only functions $\varphi_1(\cdot)$ and $\varphi_2(\cdot)$ are required, but also function $\varphi_3(\cdot)$. Finally, we observe from Fig. 7 that the lower reverse leakage currents and the higher breakdown voltages of the improved diodes yield higher EH efficiencies, and thus, are preferable for SWIPT, when the received power ρ is low and high, respectively. In the following, we will utilize the obtained EH models to design the input signal distributions and evaluate the performance of THz SWIPT systems.

C. Input Distribution, Mutual Information, and Achievable Rate

In this section, we numerically investigate the performance of THz SWIPT systems when the proposed input distributions are adopted at the TX. First, for the considered RTD designs and different peak TX amplitudes A , we determine and plot the input cdfs F_s^{opt} and F_s^{ach} obtained

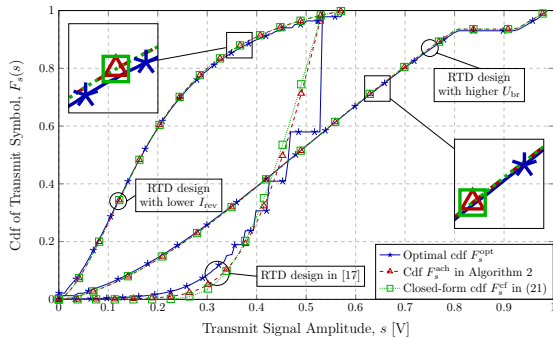
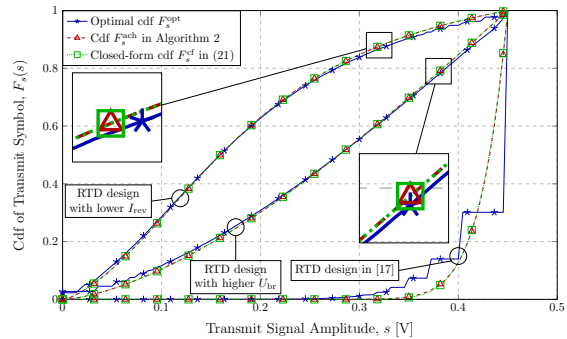
(a) High peak TX amplitude $A = 2$ V(b) Low peak TX amplitude $A = 0.45$ V

Fig. 8. Cdfs F_s^{opt} , F_s^{ach} , and F_s^{cf} obtained for different RTD designs and peak TX amplitudes A .

with Algorithms 1 and 2, respectively, in Fig. 8. Furthermore, in Fig. 8, we additionally plot the input cdfs F_s^{cf} obtained for the proposed closed-form pdf f_x^{cf} in (17). For the results shown in Fig. 8, we assume a line-of-sight channel between the TX and RX with $\hat{h} = 1$ and adopt a required average harvested power of $\bar{P}_{\text{req}} = 50 \mu\text{W}$, which is smaller than \bar{P}_{max} for all considered RTD designs. For the cdfs shown in Figs. 8(a) and 8(b), we consider high and low peak transmit amplitudes of $A = 2$ V and $A = 0.45$ V $\leq \frac{\sqrt{\rho_{\text{max}}}}{|h|}$, respectively.

First, from Fig. 8, we observe that the suboptimal cdfs F_s^{ach} , which maximize the achievable rates $J_{\bar{F}_x}^*$, and the proposed closed-form cdfs F_s^{cf} are almost identical for all considered RTD designs and all considered values of A . Next, we observe that in contrast to F_s^{ach} and F_s^{cf} , the cdf F_s^{opt} is partially piecewise constant since for SWIPT systems with bounded input alphabets, the optimal input distributions are discrete [4], [14]. Moreover, we note that if the peak TX amplitude A is high, the maximum transmit signal amplitude \bar{A} is determined by the maximum harvested power ρ_{max} , which is lower for the RTD developed in [16] compared to the improved RTD designs, as shown in Fig. 7. Finally, we observe that for the lower peak TX amplitude A , significantly higher transmit signal amplitudes are preferable for the RTD design in [16] compared to the improved RTDs. This is due to the lower EH efficiency and the lower maximum harvested power of the RX circuit equipped with the RTD developed in [16], see Fig. 7.

In Fig. 9, for the derived input pdfs, we plot the mutual information obtained for different RTD designs and different required average harvested powers \bar{P}_{req} . In particular, for the pdf f_s^{opt} obtained with Algorithm 1, we first calculate the mutual information $I_s(f_s^{\text{opt}})$ in (6). Next, for the pdf f_s^{ach} determined with Algorithm 2, we find the maximum achievable information rates $J_x(f_x^{\text{ach}}) = J_{\bar{F}_x}^*$ and the corresponding mutual informations $I_s(f_s^{\text{ach}})$ in (6) with the output pdf

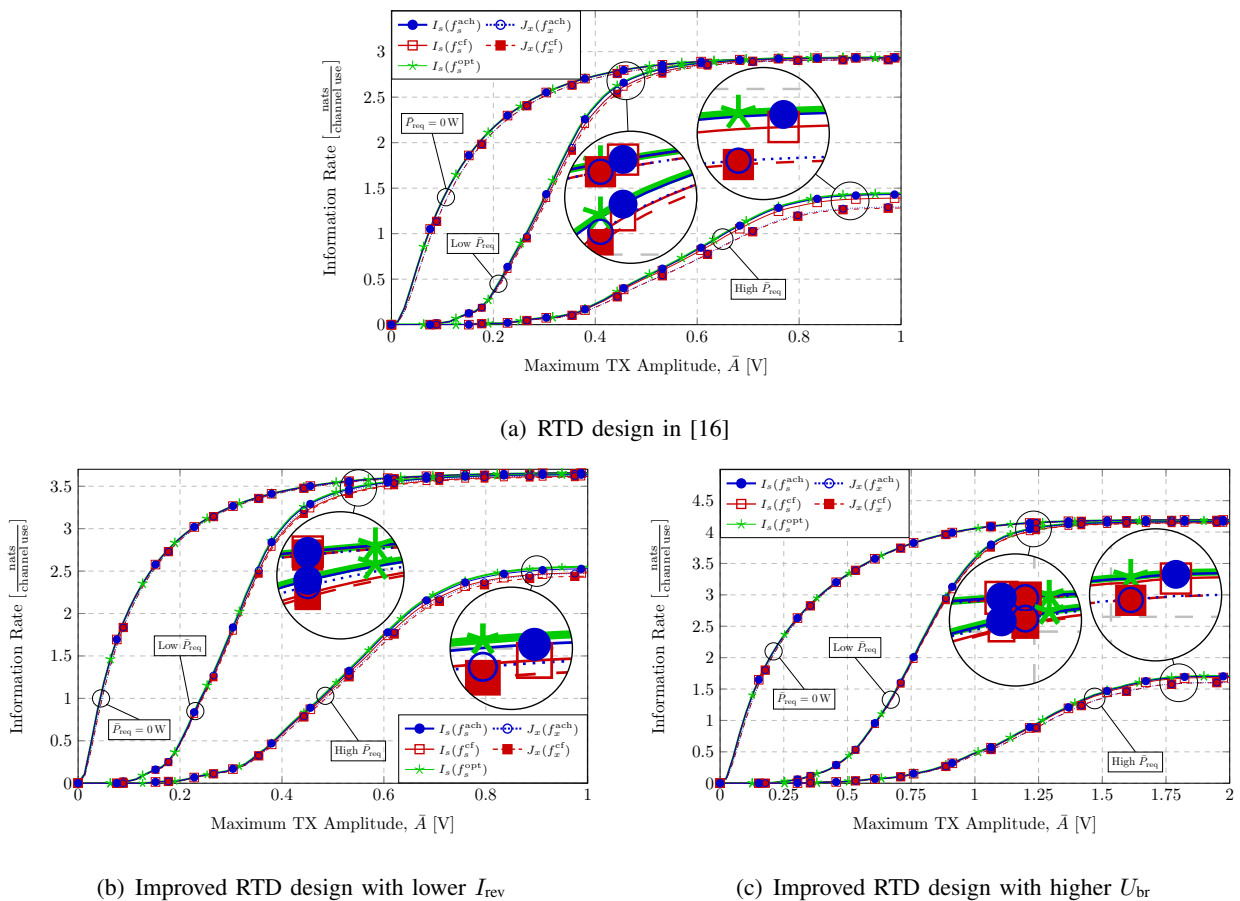


Fig. 9. Mutual information and achievable rate for different input distributions, required average harvested powers \bar{P}_{req} , and maximum transmit signal amplitudes \bar{A} .

f_y^{ach} defined in Corollaries 1 and 2. Finally, for the proposed closed-form pdf f_x^{cf} , the achievable rate $J_x(f_x^{\text{cf}})$ is provided in Proposition 5 and the corresponding mutual information $I_s(f_s^{\text{cf}})$ is given by (6). For the results in Figs. 9(a), 9(b), and 9(c), we consider the cases, where the RX circuit is equipped with the RTD design proposed in [16], the RTD design with improved I_{rev} , and the RTD design with improved U_{br} , respectively. Furthermore, for each considered RTD design, we study the performance of a pure wireless information transfer system with $\bar{P}_{\text{req}} = 0$ and a THz SWIPT system with low and high required average harvested powers of $\bar{P}_{\text{req}} = 0.4\hat{P}_{\text{max}}$ and $\bar{P}_{\text{req}} = 0.8\hat{P}_{\text{max}}$, respectively, where $\hat{P}_{\text{max}} = \max_{\rho \in [0, \rho_{\text{max}}]} \psi(\rho)$ is the maximum harvested power at the RX.

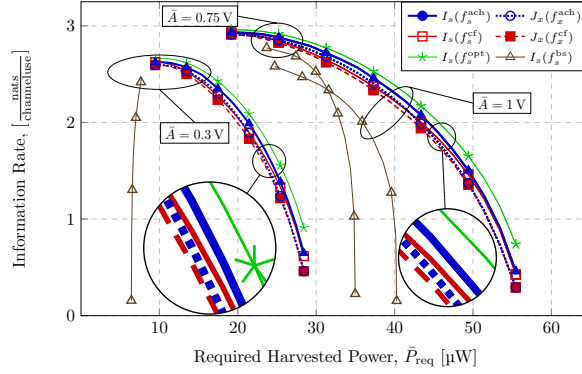
First, we observe from Fig. 9 that due to higher EH efficiencies, RX circuits equipped with the improved RTD designs significantly outperform the EH circuits employing the RTD design in [16]. Next, we note that for pure wireless information transfer with $\bar{P}_{\text{req}} = 0$, as expected, both proposed pdfs f_s^{ach} and f_s^{cf} yield the maximum achievable information rate $J_{\mathcal{F}_x}^*$. Furthermore, for

all considered values of \bar{P}_{req} , the maximum mutual information $I_s(f_s^{\text{opt}})$ is only slightly higher than the mutual information and achievable rate obtained with the proposed suboptimal pdfs f_s^{ach} and f_s^{cf} . Moreover, since there is no tradeoff between the achievable rate and harvested power for low power ratios $\frac{\bar{P}_{\text{req}}}{\bar{P}_{\text{max}}} \leq \frac{1}{3}$, see Proposition 3, we observe in Fig. 9 that as the maximum TX amplitude $\bar{A} \rightarrow \infty$, the achievable rate and mutual information obtained for low values of \bar{P}_{req} are identical. Finally, we note that for low TX amplitudes \bar{A} and high harvested powers \bar{P}_{req} , the values of $I_s(\cdot)$ and $J_x(\cdot)$ depend on both \bar{A} and \bar{P}_{req} , and hence, in this case, there is a tradeoff between the mutual information and the average harvested power that will be investigated in the next section.

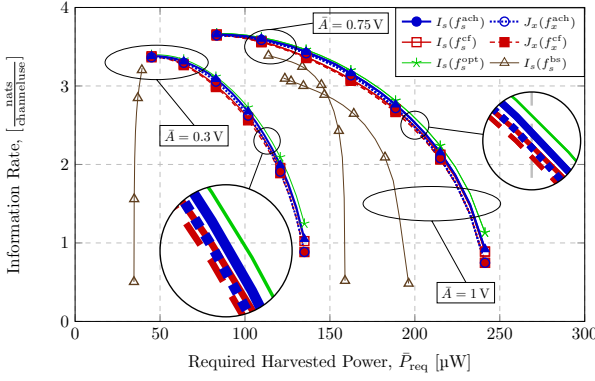
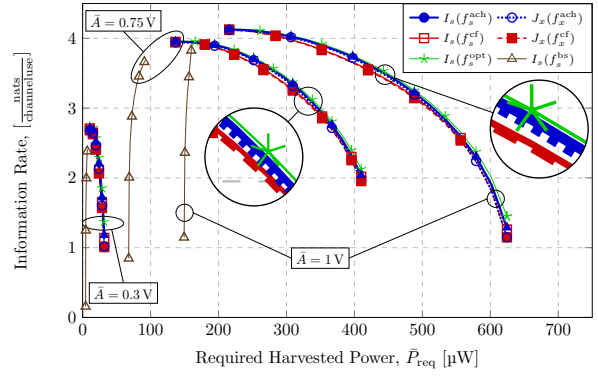
D. Optimal and Achievable Rate-Power Tradeoffs

In the following, we analyze the rate-power tradeoff of THz SWIPT systems. To this end, in Fig. 10, we plot the mutual information, achievable rate, and average harvested power for different values of the maximum amplitude of the transmitted signal \bar{A} and different RTD designs. In particular, for different values of required harvested power $\bar{P}_{\text{req}} \in [0, \frac{1}{3}\bar{P}_{\text{max}}]$ and $\bar{P}_{\text{req}} \in [\frac{1}{3}\bar{P}_{\text{max}}, \bar{P}_{\text{max}}]$, we calculate the mutual informations $I_s(\cdot)$ and achievable rates $J_x(\cdot)$ for the derived optimal input pdf f_s^{opt} and the proposed suboptimal pdfs f_s^{ach} and f_s^{cf} . Also, as a baseline scheme, we adopt centered Gaussian transmit symbols with pdf $f_s^{\text{bs}} = \frac{\mathcal{N}(\frac{2s-\bar{A}}{2\sigma_s})}{\sigma_s \text{Erf}(\frac{\bar{A}}{2\sqrt{2}\sigma_s})}$ with support $[0, \bar{A}]$, where $\mathcal{N}(x) = \frac{1}{\sqrt{2\pi}} \exp(-\frac{x^2}{2})$ is the pdf of the standard Gaussian distribution and $\text{Erf}(\cdot)$ is the error function [26]. In particular, for a given value of \bar{A} , the corresponding values of mutual information $I_s(f_s^{\text{bs}})$ and average harvested power $\bar{P}_s(f_s^{\text{bs}})$ are obtained by adjusting the variance σ_s of the truncated Gaussian f_s^{bs} .

First, as in Fig. 9, we observe in Fig. 10, that for any maximum transmit signal amplitude \bar{A} , the improved RTD designs yield higher information rates than the RTD design in [16]. Next, we note that for any given required average harvested power \bar{P}_{req} and for each RTD design, the proposed SWIPT system is able to achieve a significantly higher mutual information than the baseline scheme, and thus, Gaussian signals are highly suboptimal for THz SWIPT. Furthermore, as in Fig. 9, we observe also in Fig. 10 that for all \bar{A} and \bar{P}_{req} , the gaps between mutual information $I_s(f_s^{\text{opt}})$, $I_s(f_s^{\text{ach}})$, and $I_s(f_s^{\text{cf}})$ and achievable rates $J_x(f_x^{\text{ach}})$ and $J_x(f_x^{\text{cf}})$ are small. Since the achievable rate $J_x(\cdot)$ and the mutual information $I_s(\cdot)$ decrease as the required average harvested power \bar{P}_{req} increases, see Fig. 9, for any \bar{A} , there exists a tradeoff between the mutual information $I_s(\cdot)$ /achievable information rate $J_x(\cdot)$ and the average harvested power



(a) RTD design in [16]

(b) Improved RTD design with lower I_{rev} (c) Improved RTD design with higher U_{br} Fig. 10. Optimal and achievable rate-power regions for different values of \bar{A} and RTD designs.

$\bar{P}_s(\cdot)$, respectively, that is characterized by the rate-power regions in Fig. 10. Moreover, we note that for low maximum transmit signal amplitudes, which satisfy $\bar{A} < \frac{\sqrt{\rho_1}}{|h|}$, both the mutual information and the harvested power grow with \bar{A} . However, if the maximum received power at the RX satisfies $\bar{A} \geq \frac{\sqrt{\rho_1}}{|h|}$, i.e., for $\bar{A} \in \{0.75 \text{ V}, 1 \text{ V}\}$ in Fig. 10, the boundaries of the rate-power regions obtained for the RTD design in [16] and the RTD with improved I_{rev} do not change. In this case, the tradeoff between the mutual information and average harvested power of the THz SWIPT system is determined by the maximum instantaneous harvested power $\psi(\rho_1)$ and not by the value of \bar{A} . On the contrary, for the RTD with improved U_{br} , whose ρ_1 and ρ_{max} are higher, the mutual information and harvested power grow for $\bar{A} > 0.75$. Thus, we conclude that both optimal transmit signal waveform design and careful RX circuit design are needed for efficient THz SWIPT.

VI. CONCLUSIONS

In this work, we studied THz SWIPT systems, where the RXs were equipped with RTD-based EH circuits to extract both information and power from the received unipolar ASK-modulated signal. To characterize the output power at the RX, we proposed a general non-linear piecewise EH model, whose parameters were tuned to fit circuit simulation results. Next, we derived the TX signal pdf that maximizes the mutual information between the TX and RX signals subject to constraints on the average harvested power at the RX and the peak signal amplitude at the TX. Since the computational complexity of this pdf may be high in practice, for high and low required average harvested powers, we also obtained the input pdfs maximizing the achievable information rate, which depend on the ratio between the required and maximum harvested powers. Based on this observation, we proposed a closed-form input pdf that yields a suboptimal solution of the problem. Our numerical results demonstrated that a lower reverse current flow and a higher breakdown voltage of the employed RTD are preferable if the input signal power at the RX is low and high, respectively. Furthermore, we observed that all proposed input pdfs yield similar THz SWIPT performance and significantly outperform a baseline scheme based on non-negative Gaussian transmit signals. Finally, we showed that for low and high RX powers, the rate-power tradeoff depends on the peak TX amplitude and the maximum instantaneous harvested power, respectively.

APPENDIX A: PROOF OF PROPOSITION 1

We note that for a given maximum transmit signal amplitude \bar{A} , the instantaneous harvested power can not exceed \bar{P}_{\max} . Then, the average power harvested at the RTD-based RX is upper-bounded by $\max_{f_s \in \mathcal{F}_s} \bar{P}_s(f_s) = \bar{P}_{\max}$. Thus, for any $\bar{P}_{\text{req}} > \bar{P}_{\max}$, a solution of (8) does not exist. On the other hand, for any $\bar{P}_{\text{req}} \in [0, \bar{P}_{\max}]$, there exists at least one pdf $f_s^1 = \delta(s - s_0) \in \mathcal{F}_s$ that satisfies constraint (8b) with equality, where $s_0 \leq \bar{A}$ is chosen such that $\psi(|hs_0|^2) = \bar{P}_{\text{req}}$. This concludes the proof.

APPENDIX B: PROOF OF PROPOSITION 2

Let us consider a distribution with pdf $f_s \in \mathcal{F}_s$, which has a mass point at $\tilde{s} \in \mathcal{S}$. We note that there exists a point $\bar{s} \notin \mathcal{S}$ and $\bar{s} \leq \tilde{s}$, that yields the same information signal $x = \sqrt{\psi(|h\bar{s}|^2)}$ as \tilde{s} , i.e., $\sqrt{\psi(|h\bar{s}|^2)} = \sqrt{\psi(|h\tilde{s}|^2)}$, as shown in Fig. 4. Thus, for any such distribution f_s , an equal or larger value of $\bar{P}_s(\cdot)$ and $I_s(\cdot)$ can be attained by removing the mass point \tilde{s} and increasing

the probability of \bar{s} by $f_s(\tilde{s})$. Since the new probability is in \mathcal{F}_s , there exists an optimal input pdf f_s^{opt} as solution of (8) that does not have mass points in \mathcal{S} . This concludes the proof.

APPENDIX C: PROOF OF LEMMA 1

The proof follows [24, Appendix A]. Specifically, we express the maximum mutual information in (9) as follows:

$$I_{\bar{\mathcal{F}}_x}^* \triangleq \max_{f_x \in \bar{\mathcal{F}}_x} I_x(f_x) = \max_{f_x \in \bar{\mathcal{F}}_x} h_y(f_x) - h_n \quad (19)$$

$$\geq \max_{f_x \in \bar{\mathcal{F}}_x} \frac{1}{2} \ln(e^{2h_x(f_x)} + e^{2h_n}) - h_n = J_{\bar{\mathcal{F}}_x}^*, \quad (20)$$

where $h_y(f_x)$ and $h_n = \frac{1}{2} \ln(2\pi e\sigma^2)$ are the differential entropies of y for a given pdf $f_x \in \bar{\mathcal{F}}_x$ and AWGN n in (6), respectively. This concludes the proof.

APPENDIX D: PROOF OF PROPOSITION 3

First, we note that if the average power constraint (9b) in the definition of $\bar{\mathcal{F}}_x$ is not present, the differential entropy $h_x(f_x)$, and hence, function $J_x(f_x)$ with $f_x \in \bar{\mathcal{F}}_x$ are maximized if the pdf of x is uniform and given by f_x^{ach} [24]. Furthermore, in this case, the maximum achievable information rate and the average harvested power can be expressed as $J_x(f_x) = J_{\bar{\mathcal{F}}_x}^*$ and $\bar{P}_{\text{req}} = \mathbb{E}_x\{x^2\} = \frac{1}{3}\bar{P}_{\text{max}}$, respectively. Thus, for $\bar{P}_{\text{req}} \in [0, \frac{1}{3}\bar{P}_{\text{max}}]$, for the maximization of $J_x(\cdot)$, constraint (9b) can be relaxed and the optimal distribution of x that yields $J_{\bar{\mathcal{F}}_x}^*$ can always be obtained. This concludes the proof.

APPENDIX E: PROOF OF COROLLARY 1

First, we express the pdf f_y^{ach} of the output signal $y = x + n$ in (7) as follows:

$$\begin{aligned} f_y^{\text{ach}}(y; f_x^{\text{ach}}) &= \int_{-\infty}^{\infty} f_x^{\text{ach}}(x) f_n(y-x) dx \\ &= \int_0^{\sqrt{\bar{P}_{\text{max}}}} \frac{1}{\sqrt{\bar{P}_{\text{max}}}} f_n(y-x) dx. \end{aligned} \quad (21)$$

Since n is a zero-mean Gaussian random variable with variance σ^2 , we have $\int_0^{\sqrt{\bar{P}_{\text{max}}}} f_n(y-x) dx = Q\left(\frac{y-\sqrt{\bar{P}_{\text{max}}}}{\sigma}\right) - Q\left(\frac{y}{\sigma}\right)$. This concludes the proof.

APPENDIX F: PROOF OF PROPOSITION 4

First, since x is a deterministic function of input signal s , we obtain $J_{\bar{\mathcal{F}}_x}^*$ for given \bar{A} and $\bar{P}_{\text{harv}}^{\text{req}} \geq \frac{1}{3}\bar{P}_{\text{max}}$ as follows:

$$J_{\bar{\mathcal{F}}_x}^* = \max_{f_x \in \bar{\mathcal{F}}_x} \frac{1}{2} \ln \left(1 + \frac{e^{2h_x(f_x)}}{2\pi e\sigma^2} \right). \quad (22)$$

Since function $J_x(\cdot)$ is monotonically increasing in $h_x(\cdot)$, for $\bar{P}_{\text{req}} \in [\frac{1}{3}\bar{P}_{\text{max}}, \bar{P}_{\text{max}}]$, the pdf $f_x \in \bar{\mathcal{F}}_x$ solving (22) is the maximum entropy distribution, i.e., f_x maximizes entropy $h_x(\cdot)$ among all pdfs $f_x \in \bar{\mathcal{F}}_x$ that satisfy $\mathcal{D}\{f_x\} \in [0, \sqrt{\bar{P}_{\text{max}}}]$ and $\mathbb{E}_x\{x^2\} \geq \bar{P}_{\text{req}}$ [24]. Exploiting the Karush–Kuhn–Tucker (KKT) conditions, it can be shown that the optimal pdf as solution of (22) is given by $f_x^{\text{ach}}(x)$ in Proposition 4. Moreover, the corresponding entropy of x is given by

$$h_x(f_x^{\text{ach}}) = - \int_x f_x^{\text{ach}}(x) \ln(f_x^{\text{ach}}(x)) dx = \mu_0 - \mu_1^2 \frac{\bar{P}_{\text{req}}}{\bar{P}_{\text{max}}}. \quad (23)$$

Finally, substituting (23) into (22), we obtain (13). This concludes the proof.

APPENDIX G: PROOF OF COROLLARY 2

To obtain (16), we express the output pdf $f_y^{\text{ach}}(y; f_x^{\text{ach}})$ as follows:

$$\begin{aligned} f_y^{\text{ach}}(y; f_x^{\text{ach}}) &= \int_0^{\sqrt{\bar{P}_{\text{max}}}} f_x^{\text{ach}}(x) f_n(y-x) dx \\ &= \int_0^{\sqrt{\bar{P}_{\text{max}}}} \frac{1}{\sqrt{2\pi\sigma^2}} \exp \left(-\mu_0 \right. \\ &\quad \left. + \mu_1^2 \frac{x^2}{\bar{P}_{\text{max}}} - \frac{(y-x)^2}{2\sigma^2} \right) dx \\ &= \mu_4^{-1} \exp \left(\frac{y^2}{\bar{P}_{\text{max}}} \frac{\mu_1^2}{\mu_4^2} - \mu_0 \right) \\ &\quad \left[Q \left(\frac{y - \mu_4^2 \sqrt{\bar{P}_{\text{max}}}}{\mu_4 \sigma} \right) - Q \left(\frac{y}{\mu_4 \sigma} \right) \right] \end{aligned} \quad (24)$$

This concludes the proof.

APPENDIX H: PROOF OF PROPOSITION 5

First, we express the entropy of random variable x , which follows pdf $f_x^{\text{cf}}(x)$ in (17), as follows:

$$\begin{aligned} h_x(f_x^{\text{cf}}) &= - \int_0^{\sqrt{\bar{P}_{\text{max}}}} \alpha \bar{P}_{\text{max}}^{-\frac{\alpha}{2}} x^{\alpha-1} \ln(\alpha \bar{P}_{\text{max}}^{-\frac{\alpha}{2}} x^{\alpha-1}) dx \\ &= - \int_0^1 (\alpha - 1) \ln y dy^\alpha - \int_0^1 \ln(\alpha \bar{P}_{\text{max}}^{-\frac{1}{2}}) dy^\alpha \end{aligned}$$

$$= \frac{\alpha - 1}{\alpha} - \ln \frac{\alpha}{\sqrt{P_{\max}}}. \quad (25)$$

Then, to obtain (18), we substitute (25) into the definition of achievable rate $J_x(f_x^{\text{cf}})$ in Lemma 1. This concludes the proof.

REFERENCES

- [1] N. Shanin, S. Clochiatti, K. M. Mayer, L. Cottatellucci, N. Weimann, and R. Schober, "Achievable rate-power tradeoff in THz SWIPT systems with resonant tunnelling diodes," *arXiv preprint arXiv:2305.03532, submitted to IEEE Global Commun. Conf*, 2023.
- [2] H. Tataria, M. Shafi, A. F. Molisch, M. Dohler, H. Sjoland, and F. Tufvesson, "6G wireless systems: Vision, requirements, challenges, insights, and opportunities," *Proc. IEEE*, vol. 109, no. 7, pp. 1166–1199, Jul. 2021.
- [3] H. Srieddeen, M.-S. Alouini, and T. Y. Al-Naffouri, "An overview of signal processing techniques for terahertz communications," *Proc. IEEE*, vol. 109, no. 10, pp. 1628–1665, Oct. 2021.
- [4] L. R. Varshney, "Transporting information and energy simultaneously," in *Proc. IEEE Int. Symp. Information Theory*, Jul. 2008, pp. 1612–1616.
- [5] R. Zhang and C. K. Ho, "MIMO broadcasting for simultaneous wireless information and power transfer," *IEEE Trans. Wirel. Commun.*, vol. 12, no. 5, pp. 1989–2001, May 2013.
- [6] Z. Rong, M. S. Leeson, M. D. Higgins, and Y. Lu, "Simultaneous wireless information and power transfer for AF relaying nanonetworks in the terahertz band," *Nano Commun. Netw.*, vol. 14, pp. 1–8, Dec. 2017.
- [7] Y. Pan, K. Wang, C. Pan, H. Zhu, and J. Wang, "Self-sustainable reconfigurable intelligent surface aided simultaneous terahertz information and power transfer (STIPT)," *IEEE Trans. Wirel. Commun.*, vol. 21, no. 7, pp. 5420–5434, Jul. 2022.
- [8] J. Kim and B. Clerckx, "Wireless information and power transfer for IoT: Pulse position modulation, integrated receiver, and experimental validation," *IEEE Internet Things J.*, vol. 9, no. 14, pp. 12 378–12 394, Jul. 2022.
- [9] B. Clerckx, R. Zhang, R. Schober, D. W. K. Ng, D. I. Kim, and H. V. Poor, "Fundamentals of wireless information and power transfer: From RF energy harvester models to signal and system designs," *IEEE J. Sel. Areas Commun.*, vol. 37, no. 1, pp. 4–33, Jan. 2019.
- [10] E. Boshkovska, D. W. K. Ng, N. Zlatanov, and R. Schober, "Practical non-linear energy harvesting model and resource allocation for SWIPT systems," *IEEE Commun. Lett.*, vol. 19, no. 12, pp. 2082–2085, Dec. 2015.
- [11] E. Boshkovska, D. W. K. Ng, L. Dai, and R. Schober, "Power-efficient and secure WPCNs with hardware impairments and non-linear EH circuit," *IEEE Trans. Commun.*, vol. 66, no. 6, pp. 2642–2657, Jun. 2018.
- [12] E. Boshkovska, D. W. K. Ng, N. Zlatanov, A. Koelpin, and R. Schober, "Robust resource allocation for MIMO wireless powered communication networks based on a non-linear EH model," *IEEE Trans. Commun.*, vol. 65, no. 5, pp. 1984–1999, May 2017.
- [13] D. Xu, V. Jamali, X. Yu, D. W. K. Ng, and R. Schober, "Optimal resource allocation design for large IRS-assisted SWIPT systems: A scalable optimization framework," *IEEE Trans. Commun.*, vol. 70, no. 2, pp. 1423–1441, Feb 2022.
- [14] R. Morsi, V. Jamali, A. Hagelauer, D. W. K. Ng, and R. Schober, "Conditional capacity and transmit signal design for SWIPT systems with multiple nonlinear energy harvesting receivers," *IEEE Trans. Commun.*, vol. 68, no. 1, pp. 582–601, Jan. 2020.
- [15] N. Shanin, L. Cottatellucci, and R. Schober, "Markov decision process based design of SWIPT systems: Non-linear EH circuits, memory, and impedance mismatch," *IEEE Trans. Commun.*, vol. 69, no. 2, pp. 1259 – 1274, Feb. 2021.

- [16] S. Clochiatti, K. Aikawa, K. Arzi, E. Mutlu, M. Suhara, N. Weimann, and W. Prost, “Large-signal modelling of sub-THz InP triple-barrier resonant tunneling diodes,” in *2020 Third Int. Workshop on Mobile Terahertz Syst. (IWMTS)*. IEEE, Jul. 2020.
- [17] S. Clochiatti, R. Schmidt, E. Mutlu, M. Dieudonne, W. Prost, D. Schreurs, and N. Weimann, “On-wafer characterization and modelling of InP resonant tunnelling diodes up to 500 GHz,” in *2022 52nd Eur. Microw. Conf. (EuMC)*. IEEE, Sep. 2022.
- [18] M. Villani, S. Clochiatti, W. Prost, N. Weimann, and X. Oriols, “There is plenty of room for THz tunneling electron devices beyond the transit time limit,” *IEEE Electron Device Lett.*, vol. 42, no. 2, pp. 224–227, Feb. 2021.
- [19] U. Tietze and C. Schenk, *Advanced Electronic Circuits*. Springer Science & Business Media, 2012.
- [20] P. Horowitz and W. Hill, *The Art of Electronics*, 2nd ed. Cambridge University Press, 1989.
- [21] The Keysight Technologies, Inc., *Electronic Design Automation (EDA) Software, Advanced Design System (ADS), Version 2017*.
- [22] C. Yi, D. Kim, S. Solanki, J.-H. Kwon, M. Kim, S. Jeon, Y.-C. Ko, and I. Lee, “Design and performance analysis of THz wireless communication systems for chip-to-chip and personal area networks applications,” *IEEE J. Sel. Areas Commun.*, vol. 39, no. 6, pp. 1785–1796, Jun. 2021.
- [23] F. Lemic, C. Han, and J. Famaey, “Idling energy modeling and reduction in energy harvesting terahertz nanonetworks for controlling software-defined metamaterials,” *IEEE J. Emerg. and Sel. Topics Circuits and Syst.*, vol. 10, no. 1, pp. 88–99, Mar. 2020.
- [24] A. Lapidoth, S. M. Moser, and M. A. Wigger, “On the capacity of free-space optical intensity channels,” *IEEE Trans. Inf. Theory*, vol. 55, no. 10, pp. 4449–4461, Oct. 2009.
- [25] P. G. Gottschalk and J. R. Dunn, “The five-parameter logistic: A characterization and comparison with the four-parameter logistic,” *Analytical Biochemistry*, vol. 343, no. 1, pp. 54–65, 2005.
- [26] P. Grover and A. Sahai, “Shannon meets Tesla: Wireless information and power transfer,” in *Proc. IEEE Int. Symp. Information Theory*, Jun. 2010, pp. 2363–2367.
- [27] S. Boyd, S. P. Boyd, and L. Vandenberghe, *Convex Optimization*. Cambridge University Press, 2004.
- [28] M. Grant and S. Boyd, “CVX: Matlab software for disciplined convex programming, version 2.0 beta (2013),” URL: <http://cvxr.com/cvx>, 2015.
- [29] J. Nocedal, *Numerical Optimization*, 2nd ed., S. J. Wright, Ed. New York, NY: Springer, 2006.
- [30] T. M. Cover and J. A. Thomas, *Elements of Information Theory*. John Wiley & Sons, 2012.